ELSEVIER

S0032-3861(96)00291-1

*Polymer* Vol. 37 No. 20, pp. 4555–4571, 1996

0032-3861/96/$15.00 + 0.00

# A structure oriented model to simulate the shear induced crystallization in injection moulded polymers: a Lagrangian approach

**C. M. Hsiung**
*University of Southwest Louisiana, Chemical Engineering Department, Louisiana Productivity Center, Lafayette, LA 70504, USA*

**and M. Cakmak* and Y. Ulcer**
*Polymer Engineering Institute, University of Akron, Akron, OH 44325, USA*
*(Received 31 August 1994; revised 2 August 1995)*

In this work a Lagrangian approach was used to simulate the crystallinity gradients in injection moulded PPS. This was done through the use of markers whose thermomechanical history was traced as they moved in the cavity. The results of the simulation are compared with our earlier experimental observations. It has been found that there is a good quantitative agreement between the experimental and calculated values of gapwise (ND–TD plane) and lengthwise (FD–ND plane) crystallinity distribution. The calculated results for morphological variables such as the thickness of crystalline layers and their overall span agreed well with the experimentally measured values. Copyright © 1996 Elsevier Science Ltd.

**(Keywords: stress induced crystallization; computer simulation modelling; injection moulding; engineering thermoplastics)**

## INTRODUCTION

Injection moulding is a most commonly used processing operation in the plastics industry. Plastic parts ranging from compact discs and notebook computer housing to automobile front-end assemblies can be manufactured by this operation. It is also one of the most complicated processing operations, that imparts high stress and rapid cooling as the polymers are formed into useful shapes. Resin properties, mould geometry and moulding conditions interact to induce a complex thermomechanical history to the resin during the forming operation. As a result the structural features and properties of the injection moulded parts are quite complicated and anisotropic, i.e. they vary with location along flow direction and with gap-wise position from the surface. This is especially true for semi-crystalline polymers.

Semi-crystalline polymers can be classified, according to the characteristics of their crystallization kinetics, into two main categories: fast crystallizing polymers [e.g. PE (polyethylene), PP (polypropylene)] and slowly crystallizing polymers [e.g. PET (polyethylene terephthalate), PPS (poly *p*-phenylene sulfide), and PEEK (poly ether ether ketone)]. Most of the fast crystallizing polymers have flexible backbones with regular structures. Their crystallization rate is so fast that the phase transformation is complete within the time scale of the fabrication and their structural formation cannot be significantly influenced by processing conditions.

On the other hand, the slowly crystallizing polymers usually have relatively rigid backbones containing aromatic groups, as a result, these polymers exhibit high transition temperatures. However, slow crystallization feature of these polymers makes the final structure of the parts highly dependent on the cooling rate, and causes them to vitrify if the latter is too fast. Another interesting feature caused by the rigid backbone of these slowly crystallizing polymers is their *stress sensitivity*: it has been observed qualitatively and to a certain extent quantitatively that stress can accelerate the crystallization process[1]. Our previous observations did demonstrate that the effect of stress is more pronounced and clearly distinguishable in the structure formation of injection moulded slowly crystallizing polymers[2–4]. These

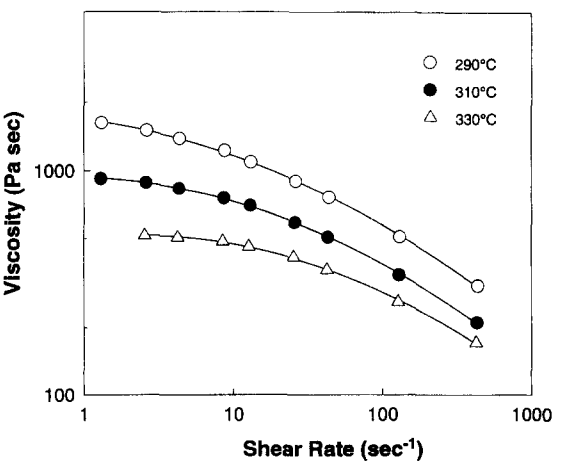


**Figure 1** Shear viscosities of PPS measured by capillary rheometer at three different temperatures

* To whom correspondence should be addressed

studies also showed that a whole spectrum of crystalline structures can be formed during the injection moulding of the slowly crystallizing polymers and their occurrence is highly dependent on the processing conditions, such as mould temperature and injection speed.

There have been many studies concerning the structure development in injection moulding of flexible chain polymers that can crystallize rapidly, including PE[5–9], PP[10–13], and POM (polyoxymethylene)[14], to name a few. These polymers generally show a highly oriented skin layer, a transcrystalline layer, and a spherulitic inner core. Crystallinity distribution in the injection moulded parts of these polymers usually increases monotonically from the skin to the core.

However, the structures of the slowly crystallizing polymers are less studied. Structure gradients in injection moulded parts of PPS, PEEK, PAEK (polyarylether ketone), and PEN (polyethylene naphthalate) have been studied by Hsiung and Cakmak[2–4] and Ulcer and Cakmak[15].

Amorphous–crystalline–amorphous multi-layer structures were observed in the gap-wise direction. These structural features were found to be very sensitive to stress effects. Similar results have also been found in injection moulding of PET, Nylon 66[16], and syndiotactic polystyrene[17].

There have been considerable experimental[18,19] and simulation[20–23] efforts to investigate the thermomechanical

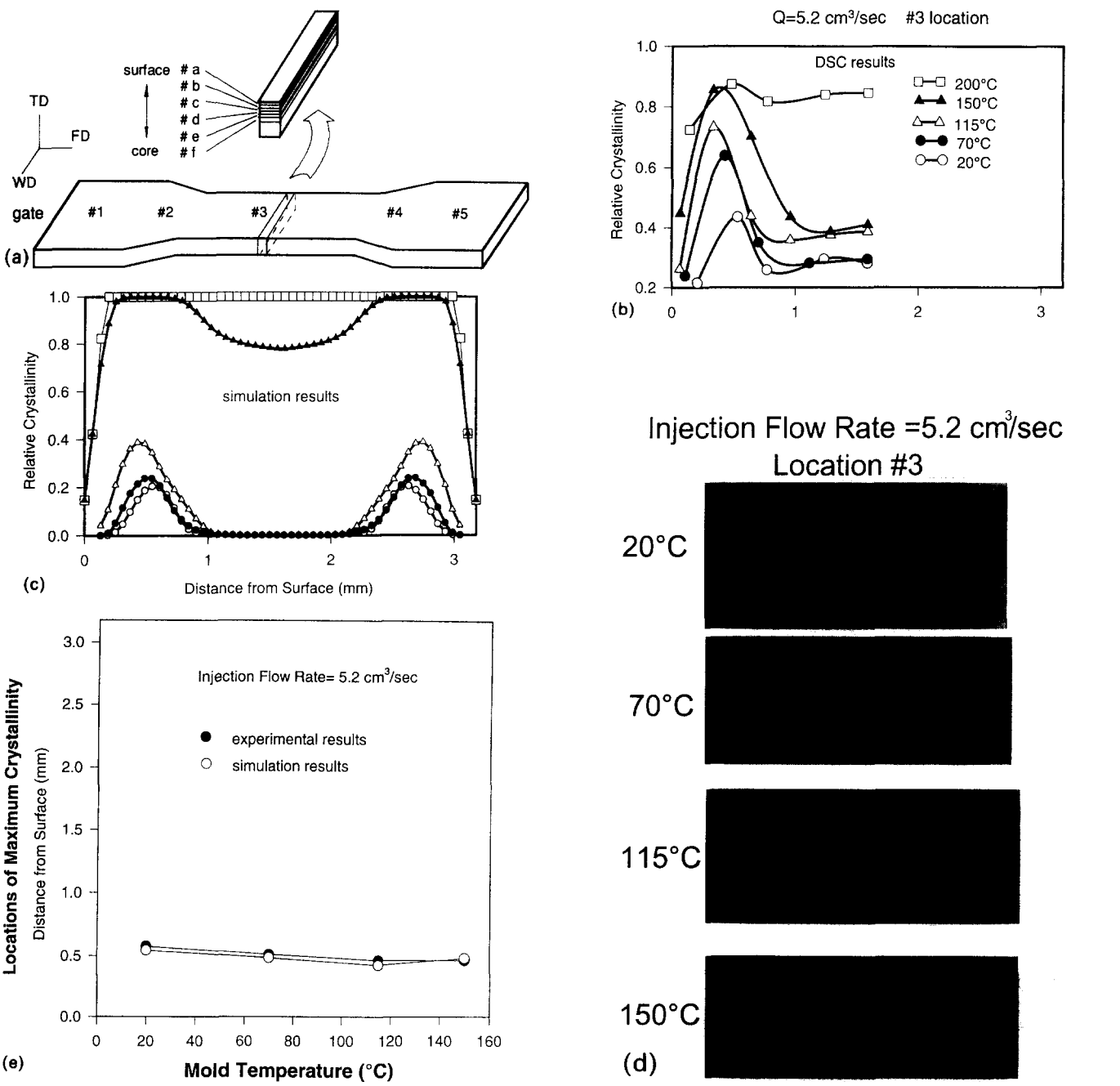


**Figure 2** (a) Schematic drawing showing the cutting method to obtain d.s.c. samples for crystallinity measurement at location #3. (b) Experimentally determined crystallinity variation along the gap-wise direction of PPS at #3 location (top) and calculated gap-wise crystallinity distribution of PPS at #3 location (bottom). (c) Calculated gap-wise crystallinity distribution of PPS at #3 location (bottom). (d) Optical photomicrographs of PPS cut perpendicular to flow direction at #3 location showing the effects of mould temperature. (e) Comparison of the locations of maximum crystallinity in gap-wise direction as measured by optical method and calculated by the simulation model (at #3 location)

aspects of mould filling of amorphous polymers such as polystyrene. Some of these studies incorporated viscoelastic models into the simulation codes[24,25]. In a later study, Rigdahl[26] incorporated residual stress distribution calculations into the calculation procedures.

Attempts to simulate the injection moulding of crystallizing polymers are rather limited. In an early report, transient temperature and crystallinity profiles within a PET slab in contact with a cooling fluid were predicted[27]. Later, Sifleet[28] mathematically modelled the unsteady state heat transfer in a crystallizing polymer during quenching. Heat transfer with crystallization during the injection moulding process was first treated in detail by a model proposed by Kamal and Lafleur[29]. This model incorporates experimentally determined crystallization kinetics parameters. Later[30–34], they adopted the White–Metzner[35] modification of the Maxwell model as their viscoelastic model and non-isothermal crystallization model of Nakamura[36] to calculate the crystallinity distribution. Recently, 2D surface crystallinity distributions of injection moulded PE have been studied by Papanasthasiou and Guell[37]. They adopted Patel and Spruiell's model for the crystallization kinetics[38]. In addition, the crystallinity distribution of POM across a rectangular part and crystallinity profile through a section have also been studied by Friedl and McCaffrey[39], where the macrokinetics approach of Malkin[40,41] was used to model the crystallization behaviour during the injection moulding process.

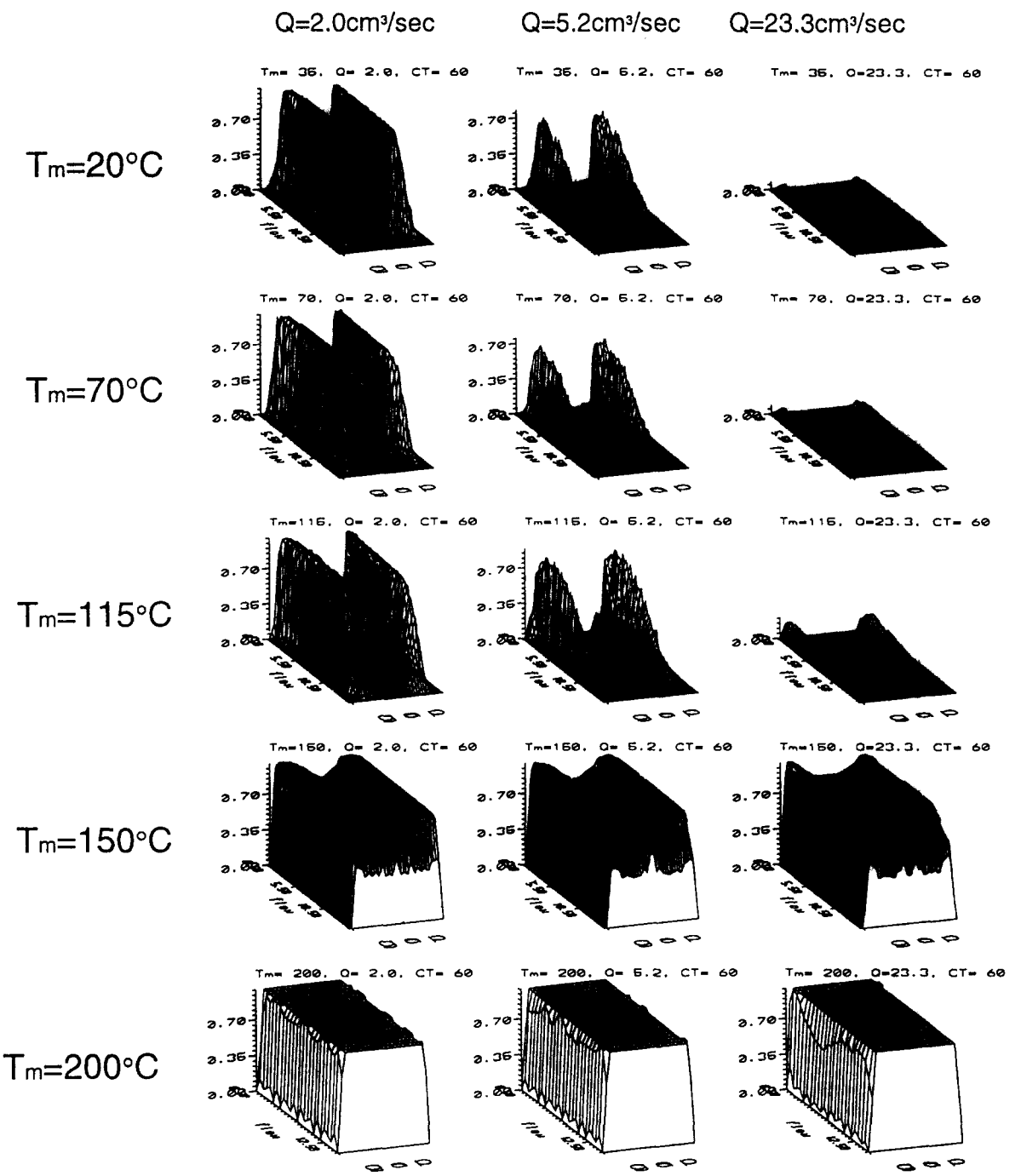


**Figure 3** Calculated crystallinity distribution in flow and gap-wise directions (FD–ND plane) inside various injection moulded PPS after a 1-min cooling time showing the effect of mould temperature and injection speed

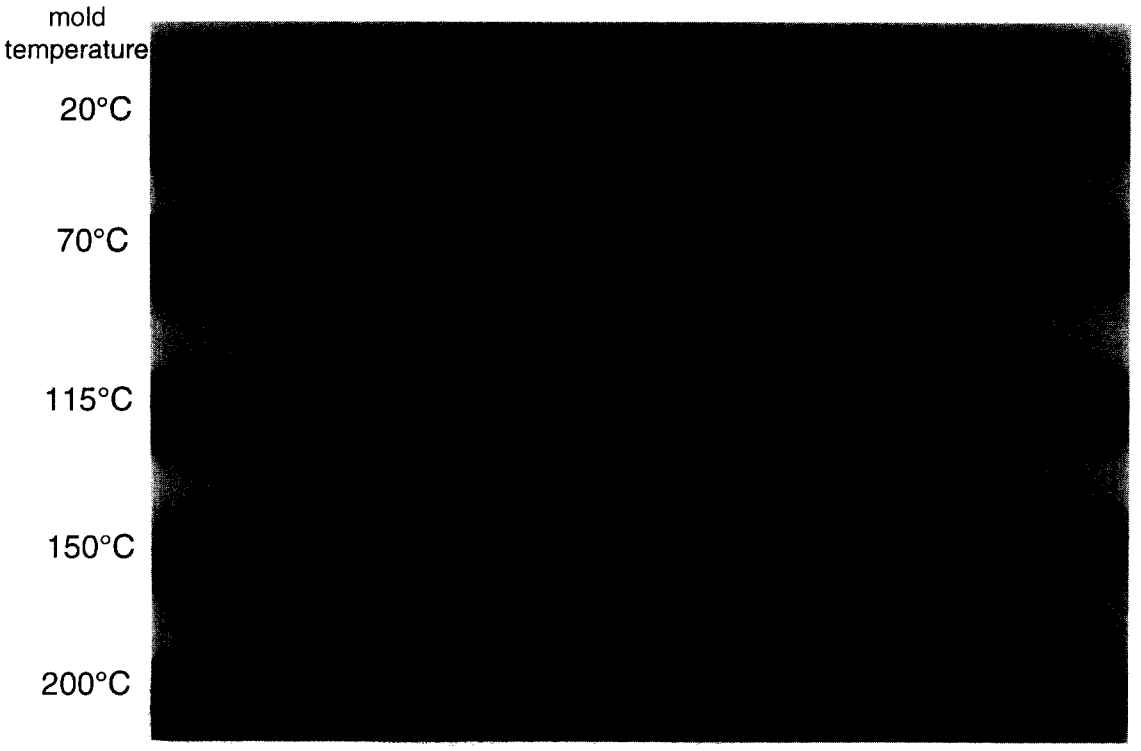


**Figure 4** Optical photomicrographs of PPS cut perpendicular to flow direction (TD–ND plane) at #3 location showing the effects of mould temperature and injection speed

Although most of the models mentioned above used non-isothermal crystallization kinetics, none of them considered stress-induced crystallization in their formulations. Furthermore, most of them studied only the fast crystallizing polymers.

Most of the early works on simulation of injection moulding dealt with 2D flow analysis[42–44]. In order to cope with cavities having complex geometry, Hieber and Shen[45] proposed a hybrid finite element/finite difference scheme in which the planar domain was discretized in terms of finite elements and the gap-wise- and time-derivatives were expressed in terms of finite differences. A similar strategy was used later by Papanasthasiou and coworkers[37,46] in order to simulate the filling of complex cavities by the boundary fitted curvilinear coordinates (BFCCs) method. They both considered a 2D flow analysis using gap-averaged melt properties and 3D transient thermal analysis. Although the strategies mentioned above are suitable for handling cavities of more general planar geometry, they sacrifice in the degree of physical details, especially in the gap-wise direction.

Since the crystallinity content of each polymer fraction inside a moulded part is a cumulative result of a nonlinear growing process that is dependent on the flow path, the only way to calculate the crystallinity distribution is to follow the flow path of each polymer fraction and calculate the crystallinity according to the temperature and stress histories that the polymer fraction has experienced. This approach has been used in the study of reaction injection moulding (RIM) and the fermentation process, where the changes in conversion or molecular weight are also a growing process[47–49].

In this study we will adopt this kind of Lagrangian approach to the 'model' we developed earlier[50] that links the stress effects to the crystallization behaviour. We will demonstrate that the model we developed is the first 'quantitative' phenomenological model that successfully links the gap between the stress and crystallization in complicated processes such as injection moulding.

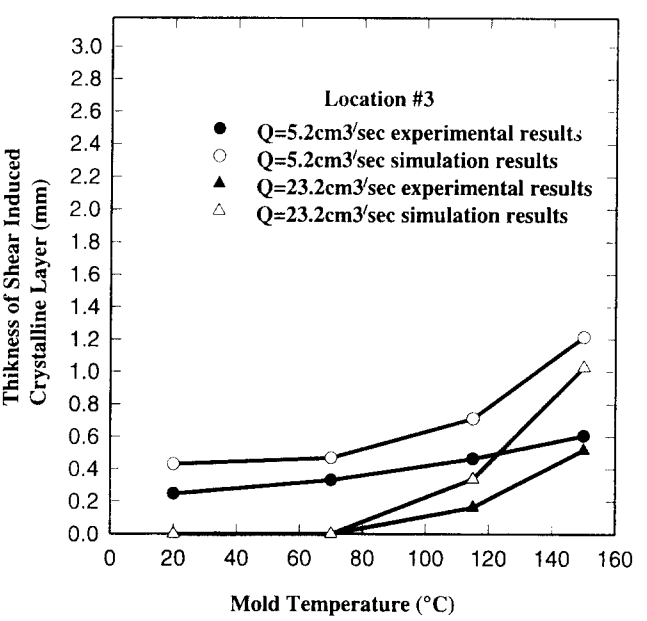


**Figure 5** Comparison of the thickness of shear induced crystalline layers as measured by optical method and calculated by simulation model (at #3 location)

## EXPERIMENTAL

The detailed procedures that led to the experimental results in this paper were described in our previous papers[2,50].

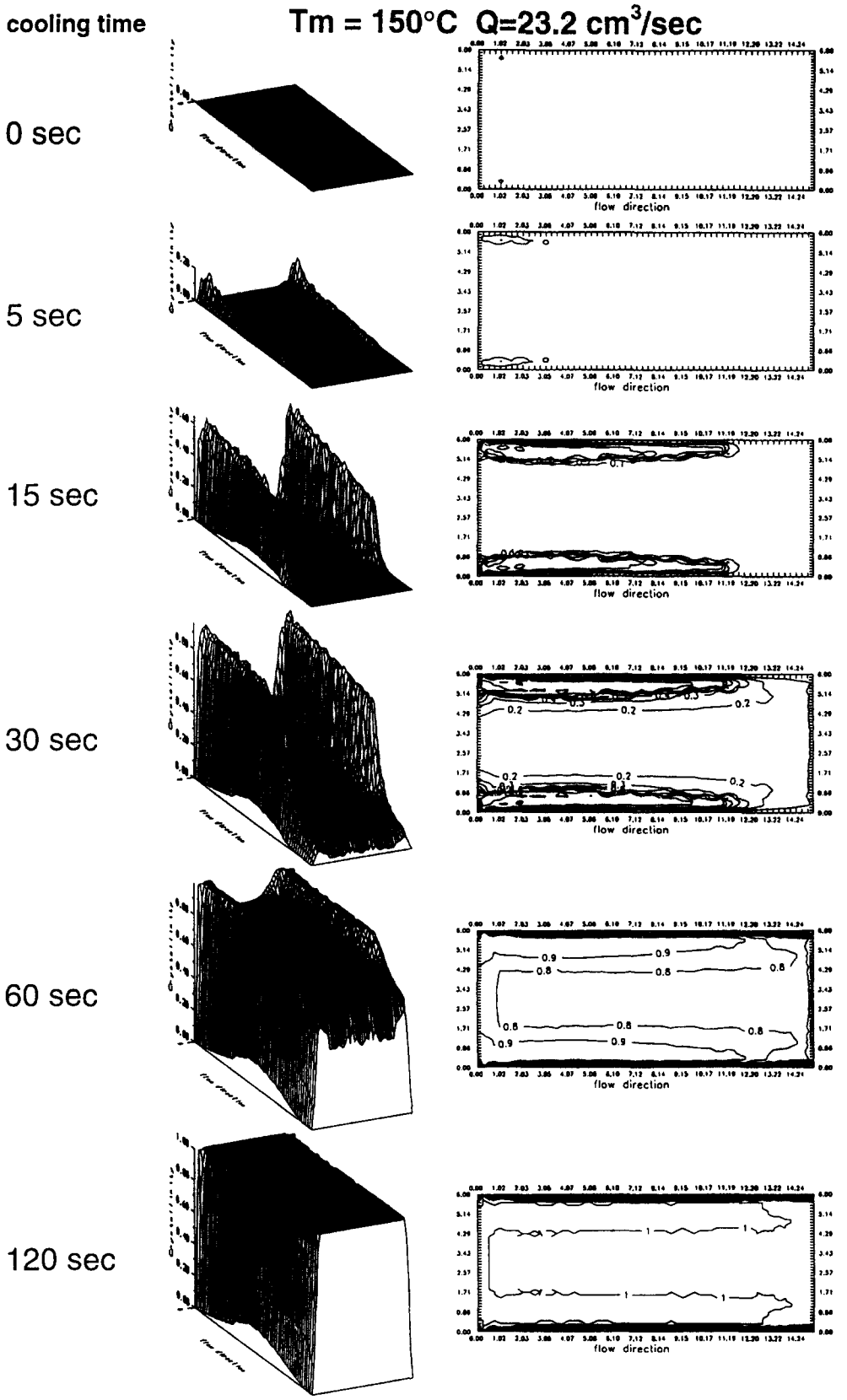


**Figure 6** Calculated crystallinity distribution (3D and contour plots) in flow and gap-wise directions inside injection moulded PPS parts showing the effects of holding time

## MATERIAL FUNCTIONS

### *Rheological equation*

For high shear and pressure processes such as injection moulding, Driscoll and Bogue[51] suggested a rheological model that incorporates all the effects of temperature, pressure, and shear rate in a single equation. In this approach, the effects of both temperature and pressure on *zero shear viscosity* were brought together by Utracki[52] through a shift factor $a_{TP}$ that is based on the free volume

factor in the Simha–Somcynsky equation of state[52,53] (S–S theory). While the effect of shear rate was correlated by a modified Cross model (*Figure 1*)

$$\eta(T,P,\dot{\gamma}) = \frac{G(P)\tau_0(T,P)}{1+a[\tau_0(T,P)\dot{\gamma}]^{\nu}} \quad (1)$$

$$G(P) = G_0(1 - 2.37 \times 10^{-3}P + 1.041 \times 10^{-4}P^2) \quad (2)$$

where $P$ is the pressure in MPa, $G_0$ is the shear modulus at the reference temperature (which is the inlet melt temperature of 310°C) and 1 atm

$$\tau_0(T,P) = \tau_0(0)\,a_{TP}(T,P) \quad (3)$$

where $\tau_0(0)$ is the zero shear time constant at the reference temperature of 310°C and 1 atm. $G_0$, $a$, $\nu$, and $\tau_0(0)$ are fitted from the viscosity vs shear rate data (see *Figure 1* and Appendix).

$$a_{TP}(T,P) = Y - Y_0 = [K1(\bar{T}) - K1(\bar{T}_0)] + [K2(\bar{T})\bar{P} - K2(\bar{T}_0)\bar{P}_0] \quad (4)$$

where $Y = 1/(1-y)$ and $y$ is the occupied volume fraction from the S–S theory[53], and the expression for $Y$ was approximated by $Y = K1(\bar{T}) + K2(\bar{T})\bar{P}$[51]. Furthermore, $K1(\bar{T})$ and $K2(\bar{T})$ can be approximated by the WLF form[51] as:

$$K_1(\bar{T}) = \frac{0.1665}{(\bar{T} - 0.01915)} \quad (5)$$

$$K_2(\bar{T}) = \frac{0.44}{(\bar{T} - 0.0224)} \quad (6)$$

where $\bar{T} = T/T^*$ and $\bar{P} = P/P^*$ are the reduced temperature and pressure, respectively, of the S–S theory with $T^* = 12\,680$ K and $P^* = 745$ MPa.

*Thermo-physical properties*

Specific heat without considering crystallization $C_p'$ was experimentally determined using a DuPont 910 differential scanning calorimeter (d.s.c.). These data were incorporated into the calculation scheme as a look-up-table. Thermal conductivity $k$ and density $\rho$ are assumed to be constant at $2.88 \times 10^4$ erg cm$^{-1}$ s$^{-1}$ C$^{-1}$ and 1.3 g cm$^{-3}$ respectively[50].

*Crystallization kinetics*

The degree of crystallinity $\alpha(t)$ is calculated through[50]:

$$\alpha(t) = 1 - \exp\left[-\left(\int_{t_{cs}}^{t} K(u)\,du\right)^{n_c}\right] \quad (7)$$

where $t_{cs}$ is the starting time of crystallization, $K$ is the non-isothermal rate constant and $n_c$ is the Avrami index.

*Induction time $t_I$.* In order to determine when crystallization actually starts, i.e. the value of $t_{cs}$, we have to consider an accumulated induction time factor $\theta$ defined as[50]:

$$\theta = \int_{T_0}^{T}\left(\frac{1}{t_I}\right)dt \quad (8)$$

The crystallization will start when $\theta > 1.0$. In this equation the induction time $t_I$ is a function of both temperature and shear stress

$$\log t_I = \log t_{Ib} + D(T - T_b)^2$$
$$T_b = T_{bq} + \tau E \quad (9)$$
$$\log t_{Ib} = \log t_{Ibq} - \tau F$$

*Isothermal ultimate heat of crystallization $\lambda_\infty$.* This value was determined experimentally as a function of temperature, using d.s.c. Again it was supplied to the simulation program through a look-up-table.

*Non-isothermal rate constant $K$.* As was described in our previous paper[50], the temperature and stress dependency of $K$ can be represented by the following equations:

$$\log K = \log K_p - A(T - T_p)^2$$
$$T_p = T_{pq} + \tau B \quad (10)$$
$$\log K_p = \log K_{pq} + \tau C$$

*Avrami exponent $n_c$.* In general, higher Avrami exponents represent greater dimensionality in the crystal growth process. Here, we use an arbitrary simple linear relationship between $n_c$ and $\tau$, where $n_c$ is equal to 3.0 at quiescent state ($\tau = 0$) and decreases to approach 1.0 as shear stress increases.

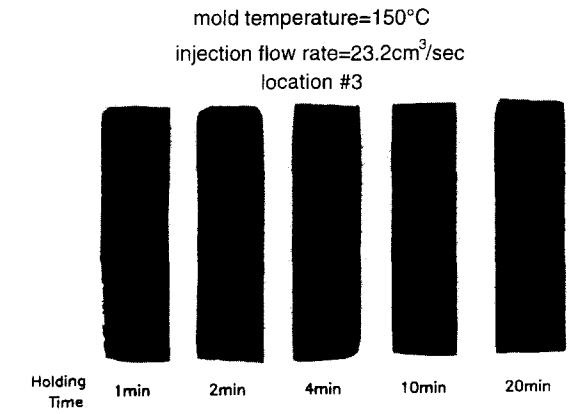


**Figure 7** Optical photomicrographs of PPS cut perpendicular to flow direction at #3 location showing the effect of holding time

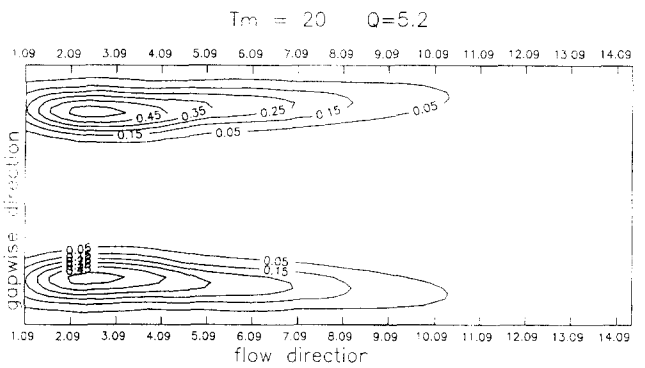


**Figure 8** Calculated crystallinity distribution (contour plot) in flow and gap-wise directions (FD–ND plane) inside the injection moulded PPS part

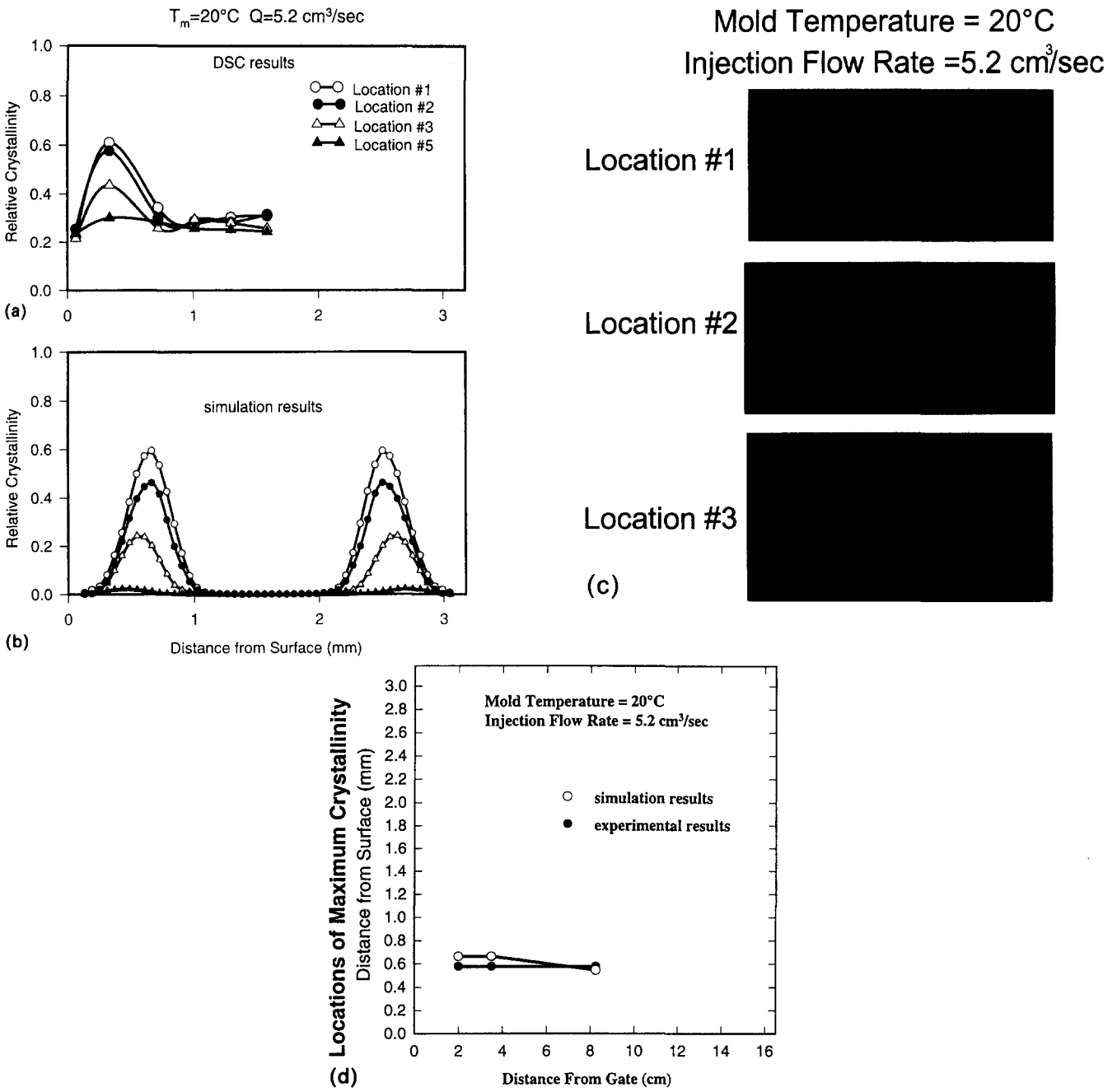


**Figure 9** (a) Experimentally determined crystallinity variation along the gapwise direction at various distances from gate (top). (b) Calculated gapwise crystallinity distribution of PPS at various distances from the gate (bottom). (c) Optical photomicrographs of PPS cut perpendicular to the flow direction at various distances from gate. (d) Comparison of the locations of maximum crystallinity in the gap-wise direction as measured by the optical method and calculated by the simulation model

Since currently there is no 'independent' technique to obtain the parameters given in phenomenological equations (9) and (10), we have estimated these parameters from the literature[1,28,36,54–59] and in our simulation work we have used these parameters for all process conditions without changing them. They are all provided in the Appendix.

## MARKERS' APPROACH

As we mentioned before, the crystallinity of polymer is an accumulative result of a nonlinear phase transformation process, and the crystallization rate is a function of temperature and stress. Since the temperature and stress are rapidly changing fields in a flowing polymer inside a cold mould, the only way to calculate the crystallinity distribution is to follow the flow path of a small unit (element) of molten polymer and calculate the crystal growth according to the temperature and stress histories it experienced (Lagrangian coordinate).

In this study the same mathematical model used in our previous simulation was considered[50]. However in this case the stress and temperature history of polymer particles was traced through 'markers'. These are hypothetical fractions of polymer melt that will keep their crystallinity integrity during the injection moulding process[60,61]. Mathematically these are array elements that store the position, local stress and crystallinity data at each time step.

In our analysis, one row of markers marches into the

inlet of the slit mould at each time interval. Once inside the mould, these markers follow the instantaneous local velocity field to move to their next locations. Then the temperature and stress histories of each marker can be traced out by following their respective flow paths. Finally, the crystallinity of each marker can be calculated based on the crystallization kinetics equations, temperature history, and stress history. The distribution of crystallinity in the injection moulded part can be traced out from the location of each marker and their respective crystallinity content.

The well-known fountain flow effect[62,63] will be considered by redirecting a fraction (in proportion to the ratio of the velocity components in the transverse and flow direction) of the markers' velocity component in the flow direction (the portion that is projected out of the melt front) to the transverse direction. As mentioned in references[47,48], as long as the fountain flow effects are considered, i.e. markers near the central region of the melt front are moved toward the wall region in a systematic way, an exact solution of the fountain flow is not necessary.

## RESULTS AND DISCUSSION

The simulation results of the injection moulding of the slowly crystallizing polymer will be discussed from three different perspectives: *the macroscopic level* (effects of processing conditions), *the individual sample level* (effect of distance from gate), and *the microscopic level* (effects along the markers' path).

### *Macroscopic level*

At this level the effects of processing conditions (mainly injection speed or injection flow rate, mould temperature, and cooling time) on the crystallinity distribution will be presented. *Figure 2a* schematically shows cutting procedures used in our experimental study of injection moulded PPS dumbbells[2] along with the locations of the slices. Crystallinity distribution characterized by the d.s.c. technique and optical photomicrographs will be compared with that predicted by the simulation program. Since in general the crystalline portion is opaque, the optical pictures of the sliced samples taken with the transmitted light source can be used to show the spatial distribution of the crystalline regions. This is not entirely true for all of this class of polymers. But our experience with PPS indicates that this is quite a reasonable assumption for this polymer.

*Figure 2b* shows the gap-wise crystallinity distribution at location #3, as characterized by d.s.c. technique whereas *Figure 2c* shows the corresponding simulation results. Results at five mould temperatures covering four distinct temperature ranges are shown in these figures. The glass transition temperature ($T_g$) of PPS is 83°C and its cold crystallization temperature $T_{cc}$ is 135°C. We chose two mould temperatures (20 and 70°C) below the $T_g$, one (115°C) between $T_g$ and $T_{cc}$ and two (150 and 200°C) in the range where thermal crystallization dominates. As can be seen from these figures, the simulation results successfully predict the two main crystalline structural features of the injection moulded parts, namely the amorphous skin-crystalline intermediate (shear)-amorphous core structure at mould temperatures from 20 to 115°C and the uniformly crystalline structure

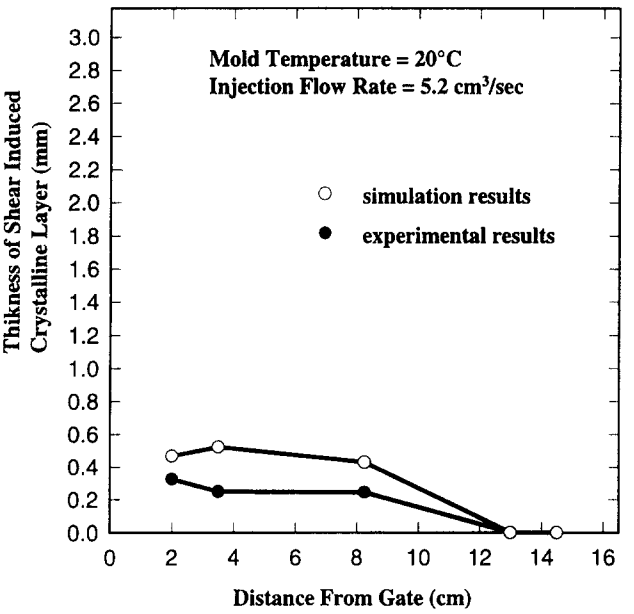


**Figure 10** Comparison of the thickness of shear induced crystalline layers as measured by optical method and calculated by simulation model

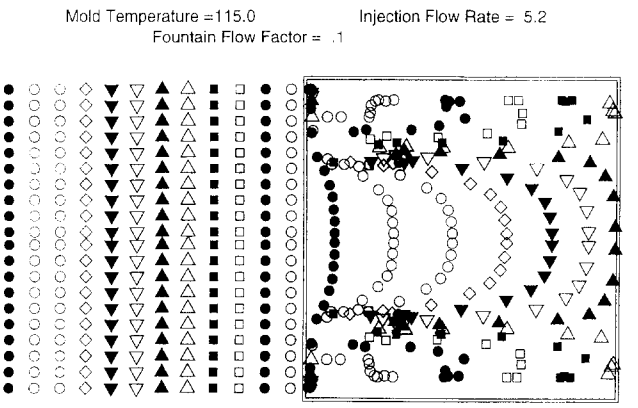


**Figure 11** Typical locations of markers before (left) and after (right) they enter the mould

at the mould temperature of 200°C. The result at 150°C, however, only shows qualitative agreement.

The accuracy of the gap-wise position of the maximum in experimentally obtained crystallinity is restricted by the thickness of the slices employed to obtain d.s.c. data (*Figure 2a*) (cf. refs 2 and 50). In our case this thickness was approximately 0.3 mm, making the exact locations of the maxima in the crystallinity profile inaccurate. In order to improve this, we have taken unpolarized optical microphotographs of these samples (shown in *Figure 2d*) and determined the darkest region which corresponds to the highest crystallinity level for this polymer. In this case there was a much better correspondence between the gap-wise position of the maxima in the simulated crystallinity profile and the actual profile (*Figure 2e*) compared to the d.s.c. data, which suffer from positional resolution problems.

The overall effect of both mould temperature and injection speed on the simulated crystallinity distribution in the FD–ND plane are shown in *Figure 3*. The experimentally observed optical microphotographs of

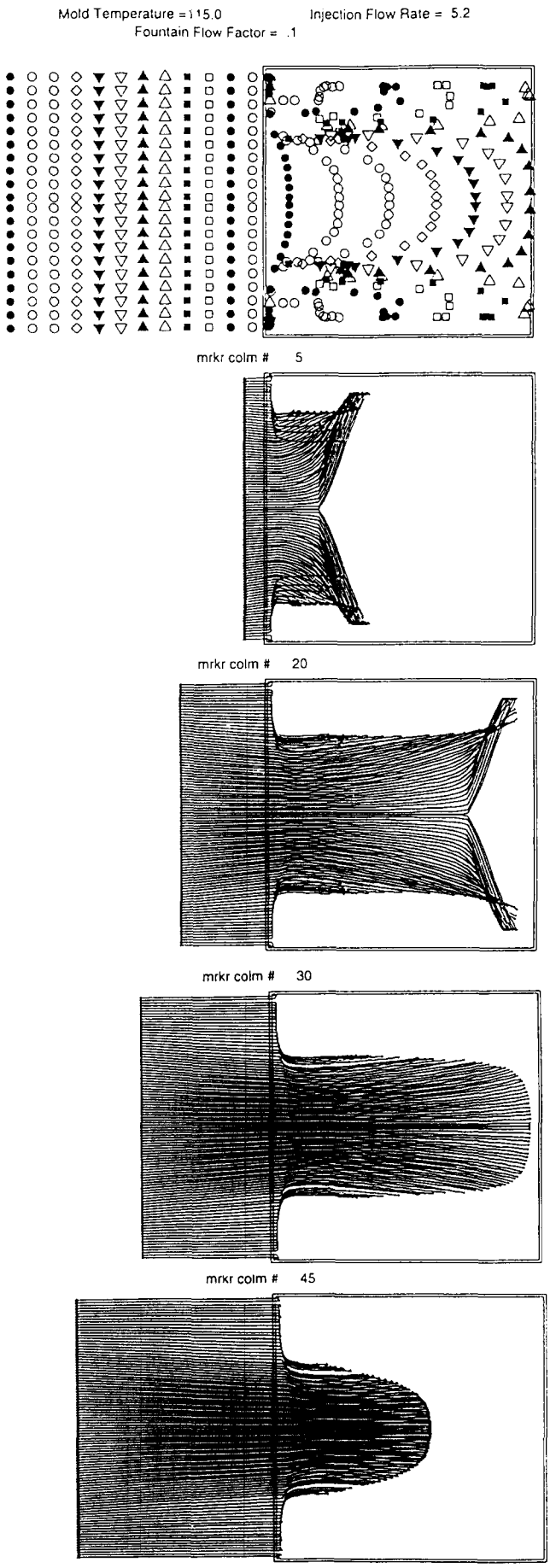


**Figure 12** Flow traces of markers belonging to marker columns that enter the mould at four different times: (a) 5th; (b) 20th; (c) 30th; and (d) 45th column

these samples sliced perpendicular to the flow direction (in the ND–TD plane) at the #3 (middle) location are shown in *Figure 4*. As we mentioned before[2], this material exhibits a spectrum of structures depending on the processing conditions including mould temperature and injection speed. These are:

(a) uniformly amorphous (or possessing small crystallinities) structure at low mould temperature and high injection speed;

(b) three layer structure gradient amorphous skin—stress crystallized ring layer—amorphous (or semicrystalline) core at intermediate mould temperatures above $T_g$ or low injection speed;

(c) uniformly crystalline parts obtained at mould temperatures well above $T_{cc}$ where the maximum rate of thermal crystallization is expected and where structural development is primarily dominated by the thermally induced crystallization.

The simulation results in *Figure 3* basically predicted the experimental results in *Figure 4* by showing clearly all the three types of structures in injection moulded PPS. However simulation predictions for the core regions of the samples moulded at the mould temperature of 150°C deviated from the experimental results. This suggested that our thermally induced crystallization kinetics should be further improved. We also measured the thickness of

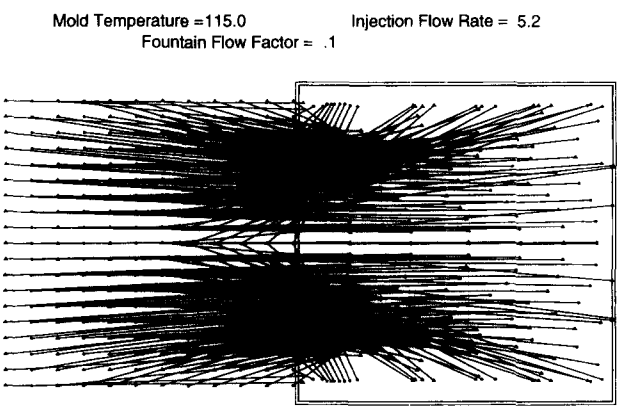


**Figure 13** Relations between the original (left) and final (right) locations of the markers as shown by connecting them with straight lines

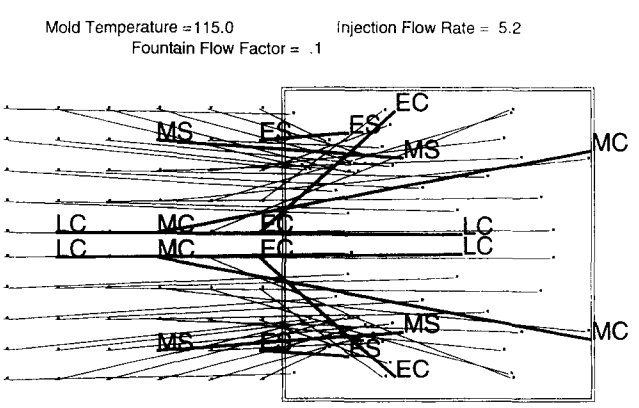


**Figure 14** Grouping of markers according to their original locations: ES, early-surface; EC, early-core; MS, middle-surface; MC, middle-core; and LC, late-core

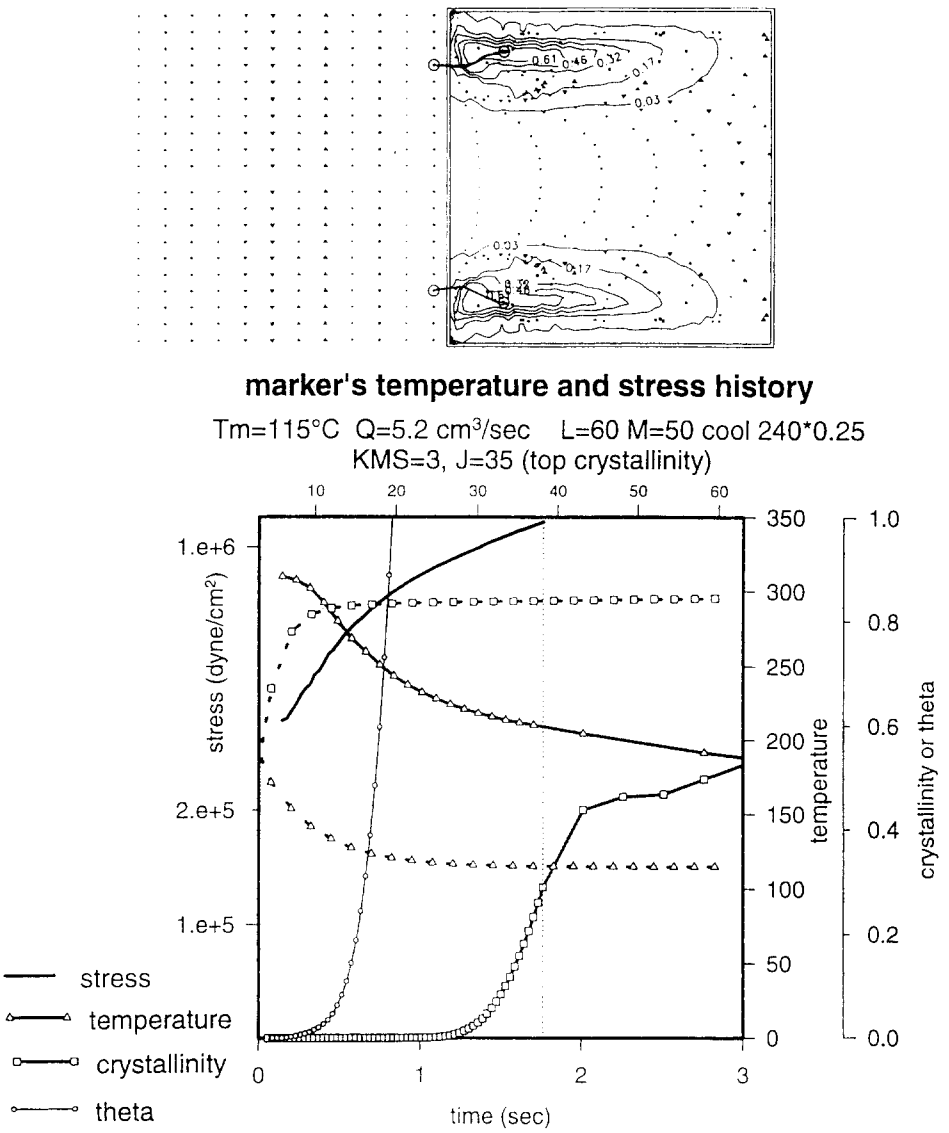


**Figure 15** ES markers' histories of stress, temperature, accumulated induction time factor ($\theta$), and crystallinity content. Solid lines vs bottom axis show the histories at early times (after the start of filling) while dashed lines vs top axis show the histories at longer times. The dotted vertical line at ca. 1.8 s shows the finish of the filling stage.

the shear induced crystalline layers optically and compared these results with the simulation results (*Figure 5*). The simulation results predicted very similar trends as the actual optical measurements, however, the predicted thickness values are slightly higher than the experimental results.

The effects of holding time on the calculated crystallinity distribution are shown in *Figure 6*. Here we choose to study this effect at the temperature where the thermally activated crystallization rates become significant (150°C). According to our preliminary isothermal crystallization kinetics studies using a d.s.c., at this temperature the half time of crystallization is around 4 min. This means that the crystallization rate is slow enough to observe the stress effects at short holding times and yet it is high enough to observe the effects of thermal crystallization at longer holding times. As can be observed in *Figures 6* and *7*, at zero holding time no crystallinity is discernible from the data. As the holding time increases the crystallinity starts to develop in those regions where significant shearing has taken place during the course of filling. Our model takes this effect into account by reducing the induction times in those regions thereby accelerating the crystallization. At later times, the whole structure gradually becomes uniformly crystalline primarily under the influence of thermally activated crystallization. The unpolarized optical transmission photographs shown in *Figure 7* clearly indicate that the shear crystallized layers appear dark as the crystallites in these regions are large enough to scatter and absorb light. The majority of transformation of structures from three layered amorphous skin + dark shear layer + amorphous core to uniformly crystalline structure within 2 min. The correlation between the photographically observed crystallinity profile development with time (*Figure 6*) and simulation results shown in *Figure 7* is quite reasonable.

*The individual sample level*

In the individual sample level we will try to confirm whether the two-dimensional distribution of crystallinity as predicted by the simulation program will match the experimentally determined results. Here we studied the gap-wise distribution of crystallinity at four characteristic locations along the flow direction, namely #1

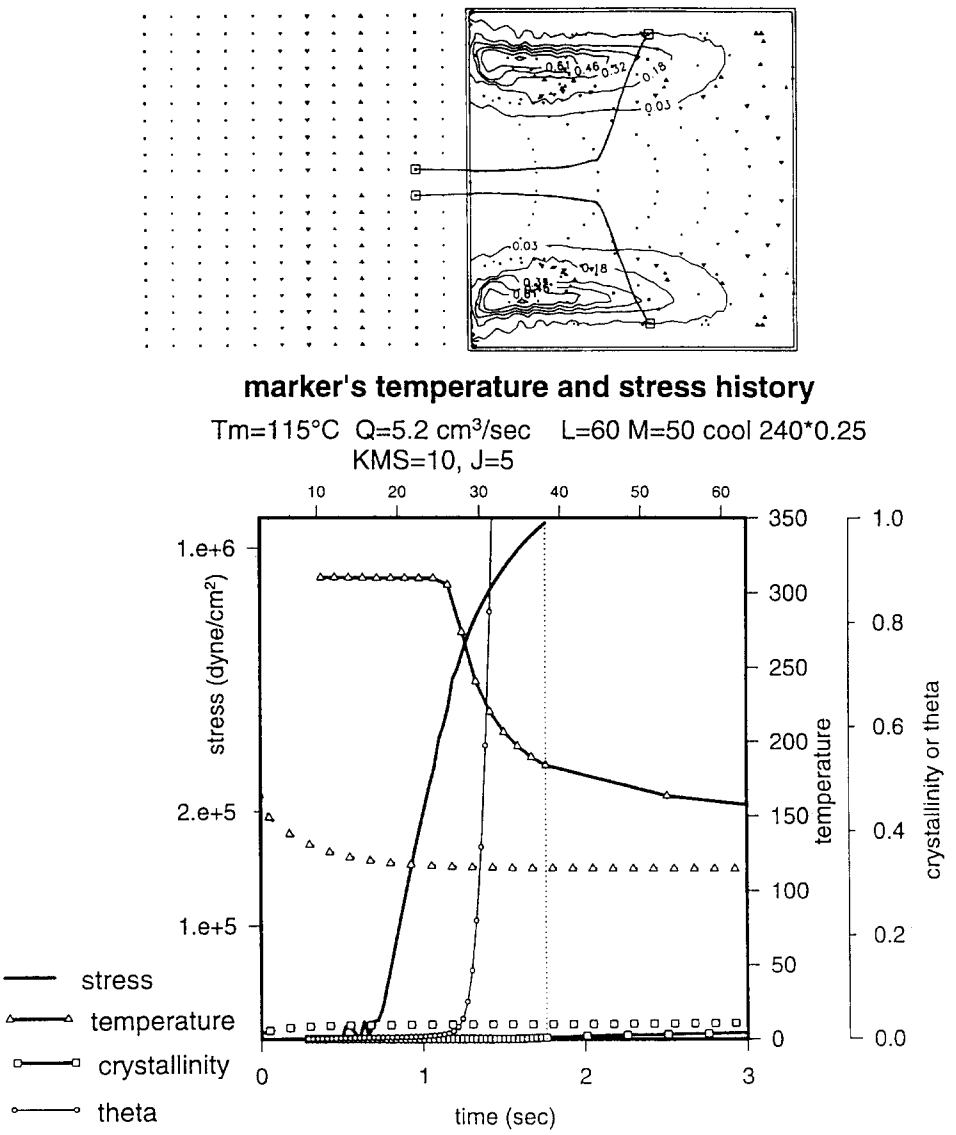


**Figure 16** EC markers' histories of stress, temperature, accumulated induction time factor ($\theta$), and crystallinity content. Solid lines vs bottom axis shows the histories at early times (after the start of filling) while dashed lines vs top axis show the histories at longer times. The dotted vertical line at ca. 1.8 s shows the finish of the filling stage.

(*close to gate*), #2 (*converging flow region*), #3 (*the middle point*), and #5 (*the end region*) (see *Figure 2d*). *Figure 8* shows the contour plot of simulated crystallinity distribution in the FD–ND plane at a mould temperature of 20°C and an injection speed of 5.2 $cm^3 s^{-1}$. Using these data the gap-wise distributions of crystallinity at distances 3, 5.5, 8, and 13 cm from the gate (#1, #2, #3, and #5 locations) are plotted at the bottom of *Figure 9a*.

For comparison, the experimental results are shown at the top of *Figure 9a*. As can be seen from these results, the simulation program predicted that the maximum crystallinity occurs at location #1 and the values of crystallinity decrease with increasing distance from the gate. The maximum degree of crystallinity predicted by simulation matched quite well with the experimental results, however, the experimentally observed minimum crystallinity values are still somewhat higher than the simulated values. Here also, the d.s.c. data suffer from the gap-wise positional resolution due to the fairly large sampling interval (compared to the simulated data). On the other hand the gap-wise position of the maximum determined from the optical photographs in *Figure 9c* are in good quantitative agreement with the simulated data (*Figure 9d*). In *Figure 10* the thickness of the shear induced crystalline layer is compared with the simulation results. Again, the simulation predicted slightly higher values than the experimental results. But the total length of the crystalline layer along flow direction was predicted quite well by the simulation.

*Microscopic level*

As we mentioned earlier, in order to trace out the thermo-mechanical histories of the individual polymer elements during the filling stage of injection moulding, we made use of hypothetical markers advancing into the mould. *Figure 11* shows a typical schematic diagram of the distribution of these markers before and after the filling process. Symbols on the left of the diagram show the initial locations of the markers while the final locations of the markers are situated inside the box on the right hand side of the diagram. The markers march into the mould one column at a time. Once inside the mould, their flow path depend on the instantaneous local velocities. They reach their final locations either when

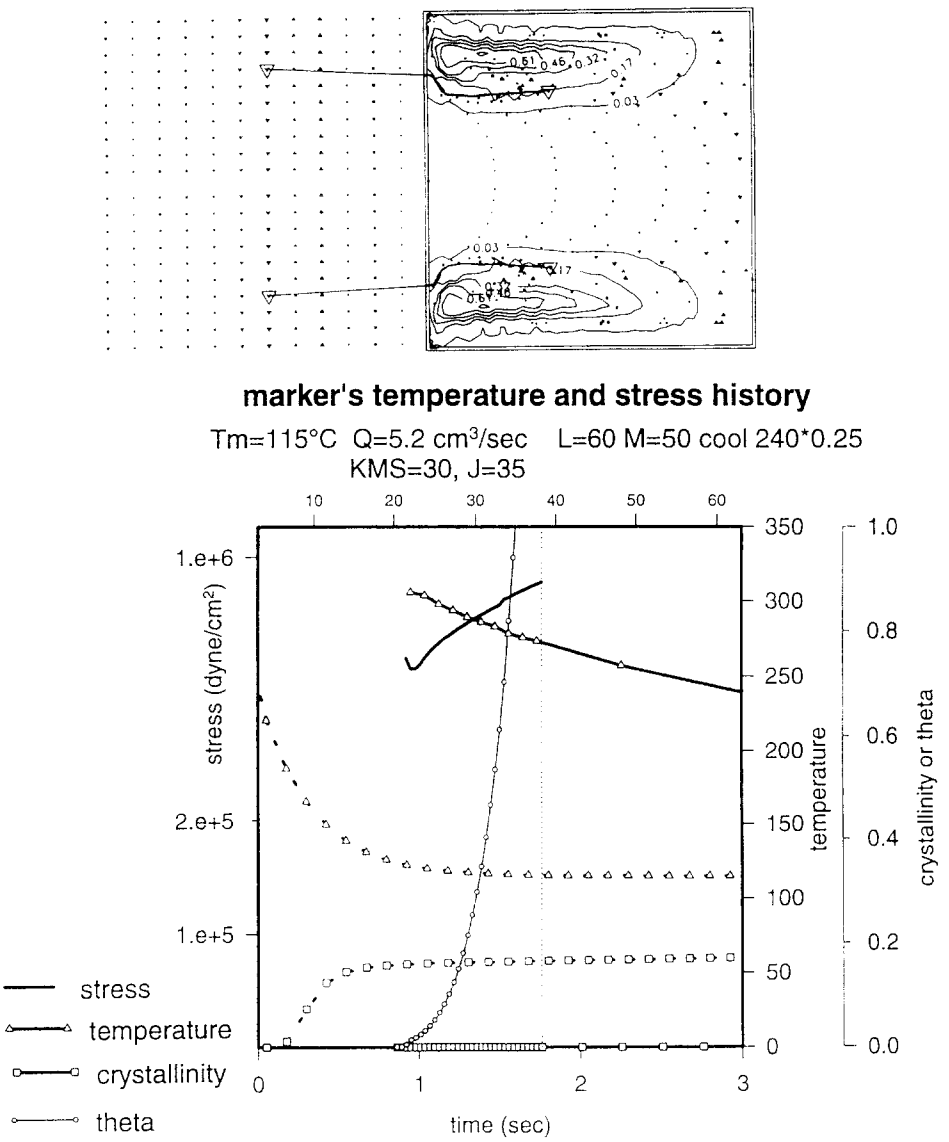


**Figure 17** MS markers' histories of stress, temperature, accumulated induction time factor ($\theta$), and crystallinity content. Solid lines vs bottom axis show the histories at early times (after the start of filling) while dashed lines vs top axis show the histories at longer times. The dotted vertical line at ca. 1.8 s shows the finish of the filling stage

they are frozen by low local temperature, or when the filling stage is finished. The final distribution of crystallinity in the injection moulded part can be traced from the final location of each marker and their respective crystallinity.

*Markers' flow path*

The flow paths of several representative marker columns are shown in *Figure 12*. In the simulation program, we used 60 columns of markers consisting of 100 markers each. *Figure 12a* shows the flow paths of the markers in the fifth column (representing polymer elements entering the mould in early stages of filling), due to the combined effect of fountain flow and rapid cooling, they have a short course in the flow direction and quickly settle at the surface region near the gate (*Figure 12a*).

In *Figure 12b* again we see that the combined effect of the fountain flow and the frozen layer spread the markers belonging to the 20th column (representing polymer elements entering the mould before the mid-filling stage) along the newly formed frozen layer. Markers at the core region of this column did travel all the way to the end corner of the mould.

The flow of the markers entering the mould at the mid-filling stage (30th column at *Figure 12c*) is restricted by the frozen layer. Like the markers at column #20, the markers entering the mould near the boundary separating the frozen layer and the flowing melt (shear zone) have a short path before they solidify and spread along the frozen layers to form the new frozen layer boundary. However, the core markers travel almost to the end of the mould while preserving their position since the filling stage finishes before they reach the melt front (fountain flow has no effect on these markers). Finally, markers that enter the mould at the final period of the filling stage (marker column #45 at *Figure 12d*) basically fill the core region near the gate of the mould and stay there since the mould is already filled.

*Classification of markers based on their flow path*

The final crystallinity distribution of the sample depends on the degree of crystallinity of each marker, and on their final locations. This, in turn, depends on the

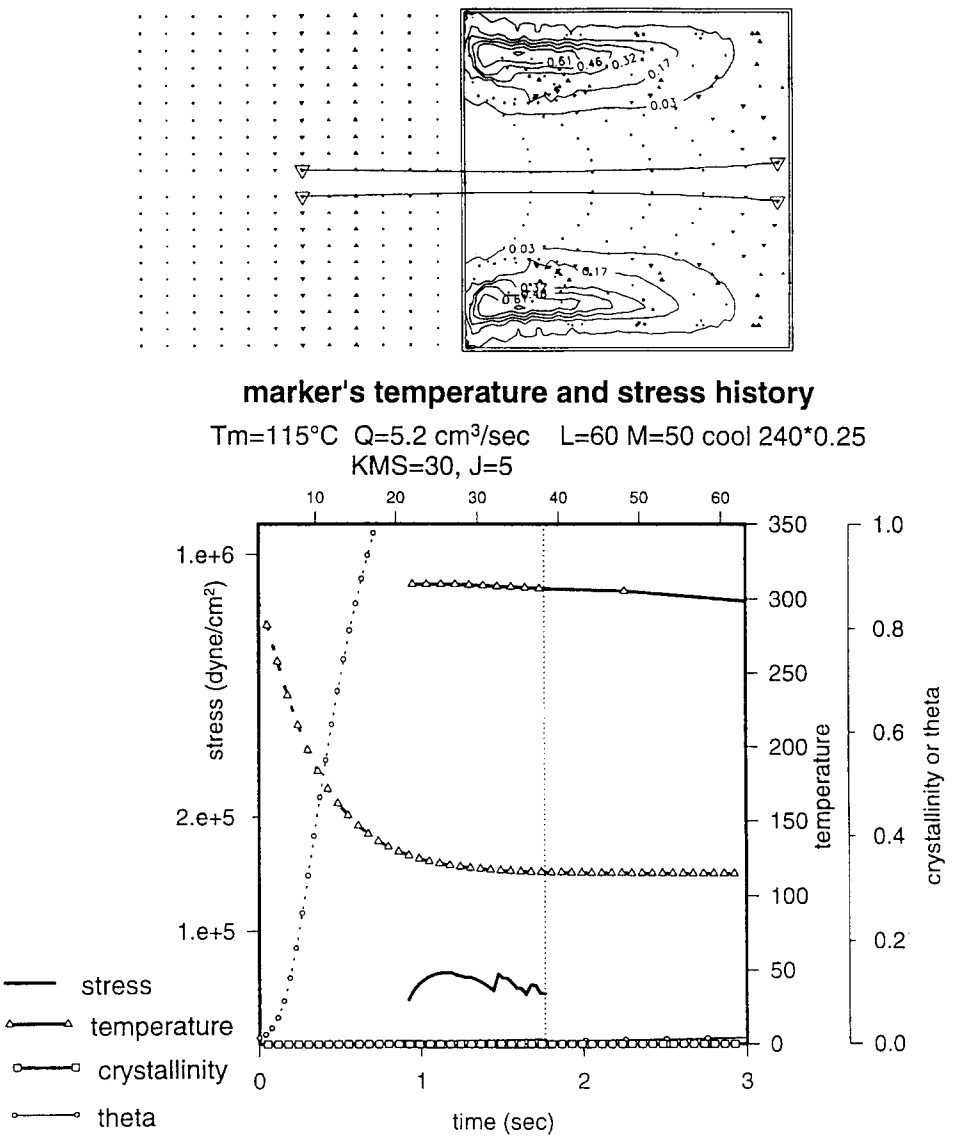


**Figure 18** MC markers' histories of stress, temperature, accumulated induction time factor ($\theta$), and crystallinity content. Solid lines vs bottom axis shows the histories at early times (after the start of filling) while dashed lines vs top axis show the histories at longer times. The dotted vertical line at ca. 1.8 s shows the finish of the filling stage

marker's flow path. However, the system is deterministic that is once we know the time and location of the marker when it enters the mould (birth ID), we can predict its flow path and final crystallinity. There are, however, 6000 markers in our analysis and each of them has a different flow path. Even if we only sketch out 4% of these markers and connect the birth place and final location of each marker (*Figure 13*) we would still be dealing with the problem of representing 240 markers each having a different flow path.

One way to deal with this problem is to make use of the flow path analysis results given in the previous section. From these results we can conclude that depending on the time (early, mid, or final) and also the locations (surface or core) at which these markers enter the mould, we can roughly classify them into five regions (*Figure 14*). They are: ES for early and surface, EC for early and core, MS for middle and surface, MC for middle and core, and finally LC for later and core. Markers from the same region basically follow a similar flow path, grow similar amounts of crystallinity, and constitute one of five characteristic regions in the final part.

*ES region*

This region consists of markers that enter the mould at early stages of filling, close to the surface or shear zone locations. The flow path of an ES marker is shown at the top of *Figure 15* together with the final distribution of the crystallinity for a sample moulded at 115°C and $5.2\,cm^3\,s^{-1}$. The final crystallinity content of this ES marker reaches a maximum value of 82%, and it resides at the shear zone near the gate. The reason why this ES marker reached the highest degree of crystallinity becomes clear when we look at its thermomechanical history (*Figure 15*). There are three main factors determining the final crystallinity content of a marker: *temperature*—in the range of 200°C the crystallization rate is fastest; *stress*—higher stress reduces the induction time and also speeds up the crystallization rate; and finally *time*—a longer shearing time causes longer shear history and thus a higher degree of crystallinity. At the bottom of *Figure 15* we show the ES marker's stress and temperature histories, accumulated induction time factor $\theta$ (cf. equation (7)), and relative crystallinity during the

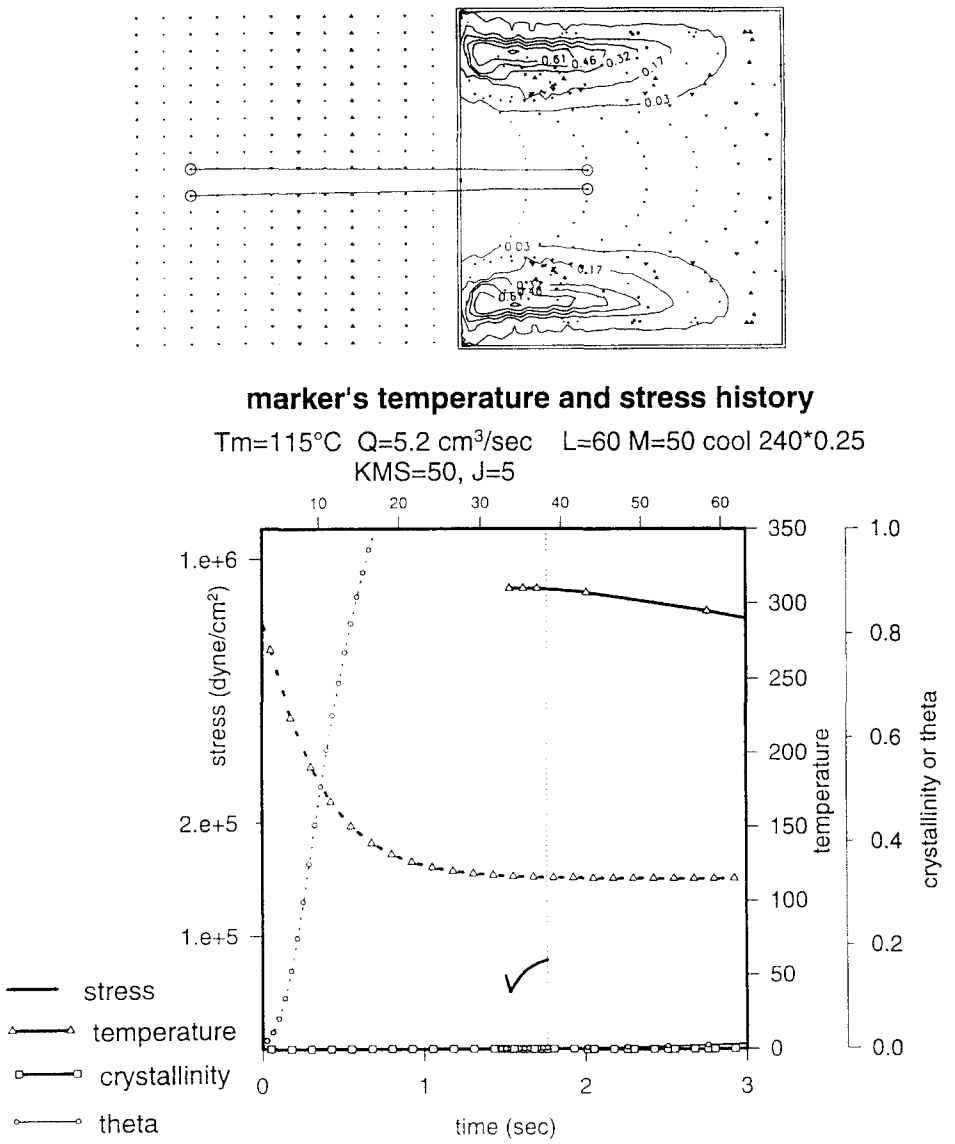


**Figure 19** LC markers' histories of stress, temperature, accumulated induction time factor ($\theta$), and crystallinity content. Solid lines vs bottom axis show the histories at early times (after the start of filling) while dashed lines vs top axis show the histories at longer times. The dotted vertical line at ca. 1.8 s shows the finish of the filling stage

filling stage. In this figure, in order to show the variation of certain variables during both the short period and the long period, two time scales are used; one for 0–3 s shown at the bottom of the figure and the other for 3–63 s shown at the top of the figure. Variables during the first time period (0–3 s) are connected by solid lines while those of the second period (3–63 s) are connected by dash lines. The vertical dotted line at 2.8 s shows the end of filling stage. As shown in this figure, the stress level this ES marker experienced during the filling stage was very high while the temperature, that was around 200°C during filling, cooled down at a very slow rate during the holding stage. Since this ES marker entered the mould at a very early stage, it also experienced a long shearing time. As we mentioned above, all three of the dominant factors (stress, temperature, and time) favour the induction and development of crystallization as marked by an early start and quick rise of the $\theta$ factor. After the $\theta$ factor reaches its final value of 1.0, the crystallinity starts to increase at a very fast rate. Substantial amount of crystallinity was achieved even before the holding stage had started. Although the crystallization rate started to slow down after the end of filling stage due to the vanishing of the shear stress, the crystallinity increased by 50% during the long period of holding stage. As can be seen from the figure, at the beginning of the holding period, the temperature was around 200°C. Hence the substantial crystallinity increase during the cooling stage was caused by the take over of the thermally induced crystallization. Markers from the ES region form the highly crystalline shear zones in the final moulded parts.

*EC region*

Markers in this region also enter the mould at early stages of filling but they are located in the core region. The flow path of an EC marker is shown at the top of *Figure 16*. Initially it moved along the hot and barely stressed core of the polymer melt until it reached the melt front. Then it moved quickly towards the surface due to the fountain flow effect. As a consequence of this, the temperature rapidly dropped to below 200°C. The stress level also started to increase rapidly. During this short period of time, $\theta$ reached 1.0 but due to the limited time

before the cessation of flow the crystallinity of the marker could not increase substantially before the end of the filling stage. During the cooling stage, since the temperature was too low, the crystallinity increased only marginally (about 3%). Markers from the EC region form the low crystallinity skin layers in the moulded parts.

*MS region*

Markers in this region enter the mould at the mid-filling stage near the surface or shear zone. The flow path of an MS marker is shown at the top of *Figure 17*. Like the ES markers the shear stress acting on the MS markers is quite high. Hence $\theta$ quickly rises above 1.0. However, since these markers enter the mould at a later stage, the shearing time is not enough for the stress induced crystallization to become significant. As a result the crystallinity does not develop during the filling stage. During the holding stage, the precursors that have been created during the filling stage crystallize as soon as the temperature reaches the rapid thermal crystallization range (170–200°C). The final crystallinity of the MS marker can then reach 17%.

*MC region*

Markers in this region entered the mould at the mid-filling stage at the core region. The flow path of the MC marker is shown at the top of *Figure 18*. During the filling stage the MC marker experienced low stresses and high temperatures. So there was no chance for crystallization of any kind to start. However, during the cooling stage, when the temperature dropped to the rapid thermal crystallization range, $\theta$ increased and eventually exceeded 1.0. But there was not enough time for the thermally induced precursors to grow, because by the time $\theta$ exceeded 1 the temperature was already too low for crystallization to proceed. Markers from the MC region thus form the amorphous end section in the moulded parts.

*LC region*

Markers in this region entered the mould at the latest period of the filling stage and near the core. The flow path of the LC marker is shown at the top of *Figure 19*. There is virtually no chance for the LC marker to initiate any kind of crystallization during the filling stage: the stress is too low, the temperature is high (supercooling is low), and the total time they spend in the mould is too short. Just like the MC marker, by the time $\theta$ exceeds 1.0, during the cooling stage, the temperature is too low for crystal growth. Markers from this MC region form the amorphous core in the moulded parts.

## CONCLUSION

In this structure-oriented injection moulding simulation program, we approach the crystallization behaviour of a slowly crystallizing polymer from a Lagrangian point of view. The flow path of each polymer fraction (marker) was traced and their thermomechanical histories were recorded along these paths to calculate the induction and growth of crystalline contents. The final crystallinity distribution of the moulded part was then evaluated based on the final locations of these markers and their respective crystallinity contents.

Three levels of study were conducted in this approach. In a macroscopic view, the effects of processing condition on the crystallinity contents were evaluated. The results of simulation match in most cases quantitatively with the experimental observations. The detailed distribution of crystallinity within a sample ($T_m = 20°C$, $Q = 5.2\,cm^3\,s^{-1}$) also confirms our simulation results. Finally the detailed mechanism of the crystallization behaviour during the injection moulding process were depicted by tracing out the histories of stress, temperature, $\theta$, and crystallinity of five representative regions of markers. From these results we concluded that the Lagrangian approach is required to successfully reproduce the phenomenological model proposed by Hsiung and Cakmak[2,3] to describe the structure formation in slowly crystallizing polymers.

## ACKNOWLEDGEMENTS

This work was primarily supported by MC's Presidential Young Investigator Award from the National Science Foundation (# DMC-8858303). CMH was supported by National Science Foundation (grant # IBN-9118094), and the Louisiana Education Quality Support Fund (Grant # LEQSF(1993-95)-RD-B-16).

## REFERENCES

1 Spruiell, J. E. and White, J. L. *Polym. Eng. Sci.* 1975, **15**, 660
2 Hsiung, C. M., Cakmak, M. and White, J. L. *Int. Polym. Proc.* 1990, **5**, 109
3 Hsiung, C. M., Cakmak, M. and White, J. L. *Polym. Eng. Sci.* 1990, **30**, 967
4 Hsiung, C. M. and Cakmak, M. *J. Appl. Polym. Sci.* 1993, **47**, 125; 149
5 Oyanagi, Y. and Yamaguchi, Y. *Res. Rep. Kogakuin Univ.* 1964, **15**, 1
6 Heise, B., Kilian, H. G., Lipke, G., Schultz, P., Woebcken, W. and Zohren, J. *Kolloid Z.* 1972, **25**, 120
7 Heckman, W. and Johnson, V. *Colloid Polym. Sci.* 1974, **252**, 826
8 Heise, B. *Colloid Polym. Sci.* 1976, **254**, 279
9 Fryer, R. E. *J. Appl. Polym. Sci.* 1979, **18**, 947
10 Kantz, M. R., Newman, H. D. and Stigale, F. H. *J. Appl. Polym. Sci.* 1972, **16**, 1245
11 Kantz, M. R. *Int. J. Polym. Mater.* 1974, **3**, 245
12 Fitchmun, D. R. and Mencik, Z. *J. Polym. Sci., Polym. Phys. Edn.* 1974, **11**, 951
13 Matsumoto, K., Miura, I. and Hayashida, K. *Kobunshi Ronbunshu* 1979, **36**, 401
14 Clark, E. S. *SPE J* 1987, **23**, 46
15 Ulcer, Y. and Cakmak, M. *SPE ANTEC Tech. Pap.* 1993, **39**, 1073
16 McCaffrey, N. J., Friedl, C. and Thomas, R. *ANTEC'90* 1990, 382
17 Miao, J., Hsiung, C. M., Cakmak, M. and Ulcer, Y. *J. Appl. Polym. Sci.* (submitted)
18 Oda, K., White, J. L. and Clark, E. S. *Polym. Eng. Sci.* 1978, **18**, 53
19 Dietz, W., White, J. L. and Clark, E. S. *Polym. Eng. Sci.* 1978, **18**, 273
20 Greener, J. and Pearson, G. H. *J. Rheol.* 1983, **27**, 115
21 Marruci, G. *Rheol. Acta* 1973, **12**, 269
22 Kamal, M. R. and Tan, V. *Polym. Eng. Sci.* 1979, **19**, 558
23 Waales, J. L. S., Van Leeuwen, J. and Vander Vigh, R. *Polym. Eng. Sci.* 1972, **12**, 358
24 Wang, K. K. Injection Molding Project, Cornell University, Progress Report #7, Oct. 1980
25 Isayev, A. I. and Hieber, C. A. *Rheol. Acta* 1980, **19**, 168
26 Rigdahl, M. *Int. J. Polym. Mater.* 1976, **5**, 43
27 Muzzy, J. D., Bright, D. G. and Hoyos, G. H. *Polym. Eng. Sci.* 1978, **18**, 437
28 Sifleet, W. *Polym. Eng. Sci.* 1973, **13** 1, 10

29 Kamal, M. R. and Lafleur, P. G. *Polym. Eng. Sci.* 1984, **24**, 692
30 Kamal, M. R. and Lafleur, P. G. *SPE ANTEC'83* 1983, 386
31 Lafleur, P. G. and Kamal, M. R. *Polym. Eng. Sci.* 1986, **26**, 92
32 Kamal, M. R. and Lafleur, P. G. *Polym. Eng. Sci.* 1986, **26**, 103
33 Browne, L. W. B. in 'Numerical Simulation of Fluid Motion', North Holland Publishing Co., 1978
34 Chu, E., Goyal, S. K. and Kamal, M. R. The SPI/SPE Plastics Show & Conference East, Philadelphia, September, 238, 1989
35 White, J. L. and Metzner, A. B. *J. Appl. Polym. Sci.* 1963, **7**, 1867
36 Nakamura, K. *J. Appl. Polym. Sci.* 1972, **16**, 1077
37 Papathanasiou, T. D. and Guell, D. C. *SPE ANTEC Tech. Pap.* 1993, **39**, 1603
38 Patel, R. M. and Spruiell, J. E. *Polym. Eng. Sci.* 1991, **30**, 730
39 Friedl, C. F. and McCaffrey, N. J. *SPE ANTEC Tech. Pap.* 1991, **37**, 330
40 Malkin, A. Y. *Polymer* 1983, **24**, 81
41 Malkin, A. Y. *Polym. Eng. Sci.* 1984, **24**, 1396
42 Lord, H. A. and Williams, G. *Polym. Eng. Sci.* 1975, **15**, 569
43 Kamal, M. R. and Kenig, S. *Polym. Eng. Sci.* 1972, **12**, 294
44 Richardson, S. M. *Rheol. Acta* 1983, **22**, 223
45 Hieber, C. A. and Shen, S. F. *J. Non-Newtonian Fluid Mechanics* 1980, **7**, 1
46 Papathanasiou, T. D. and Kamal, M. R. *SPE ANTEC Tech. Pap.* 1991, **37**, 829
47 Domine, J. D. and Gogos, C. G. *Polym. Eng. Sci.* 1980, **20**, 847
48 Manzione, L. T. *Polym. Eng. Sci.* 1981, **21**, 1234
49 Manzione, L. T. and Osinsky, J. S. *Polym. Eng. Sci.* 1983, **23**, 576
50 Hsiung, C. M. and Cakmak, M. *Polym. Eng. Sci.* 1991, **31**, 1372
51 Driscoll, P. D. and Bogue, D. C. *J. Appl. Polym. Sci.* 1990, **39**, 1755
52 Utracki, L. A. *Polym. Eng. Sci.* 1983, **23**, 446
53 Simha, R. *Macromolecules* 1977, **10**, 1025
54 Haas, T. W. and Maxwell, B. *Polym. Eng. Sci.* 1969, **9**, 225
55 Jog, J. P. and Nadkarni, V. M. *J. Appl. Polym. Sci.* 1995, **30**, 997
56 Lopez, L. C. and Wilkes, G. L. *Polymer* 1988, **29**, 106
57 Manzione, L. T. *SPE ANTEC Tech. Paper* 1987, **33**, 285
58 Lagasse, R. R. and Maxwell, B. *Polym. Eng. Sci.* 1976, **16**, 189
59 Chien, M. C. and Weiss, R. A. *Polym. Eng. Sci.* 1988, **28**, 6
60 Harlow, F. H. and Welch, J. D. *Phys. Fluids* 1965, **8**, 2182
61 Gogos, C. G. and Huang, C. F. *Polym. Eng. Sci.* 1986, **26**, 1457
62 Rose, W. *Nature* 1961, **19**, 242
63 Tadmor, Z. *J. Appl. Polym. Sci.* 1974, **18**, 1753


## APPENDIX: PARAMETERS FOR MATERIAL FUNCTIONS

### *Rheological equations*

| | |
|---|---|
| $G_0$ | 1016 Pa |
| $a$ | 0.1071 |
| $\nu$ | 0.72 |
| $\tau_0(0)$ | 1.032 s |

### *Thermal physical properties*

(a) thermal conductivity $k = 2.88 \times 10^4 (\text{erg cm}^{-1}\,\text{s}^{-1}\,{}^\circ\text{C}^{-1})$[65]

(b) density $= 1.3 (\text{g cm}^{-3})$[65]

(c) specific heat without considering crystallization $C_p'$[54]:

| Temperature (°C) | $C_p$ (J °C$^{-1}$ g$^{-1}$) |
|---|---|
| 0.0 | 1.128 |
| 84.5 | 1.261 |
| 92.0 | 1.505 |
| 2370.0 | 1.671 |
| 284.5 | 1.726 |
| 290.0 | 1.732 |
| 350.0 | 1.755 |

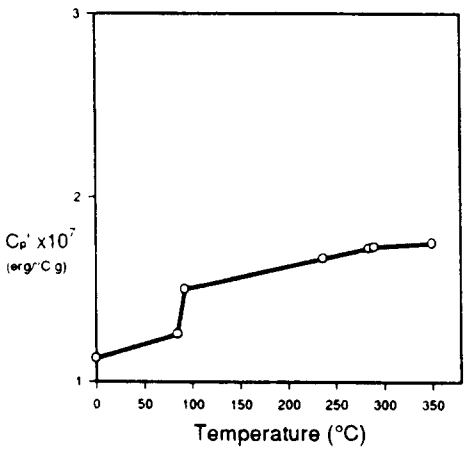


### *Crystallization kinetics*

(a) isothermal ultimate heat of crystallization[54]:

(b) induction time $t_I$[1,28,54,59,60]:

| Temperature (°C) | $\lambda_\infty$ (J g$^{-1}$) |
|---|---|
| 0 | 0.0 |
| 85 | 0.0 |
| 90 | 2.0 |
| 100 | 20.0 |
| 110 | 30.0 |
| 120 | 36.0 |
| 140 | 42.0 |
| 160 | 45.0 |
| 240 | 45.0 |
| 260 | 40.0 |
| 270 | 30.0 |
| 275 | 10.0 |
| 280 | 0.0 |
| 350 | 0.0 |

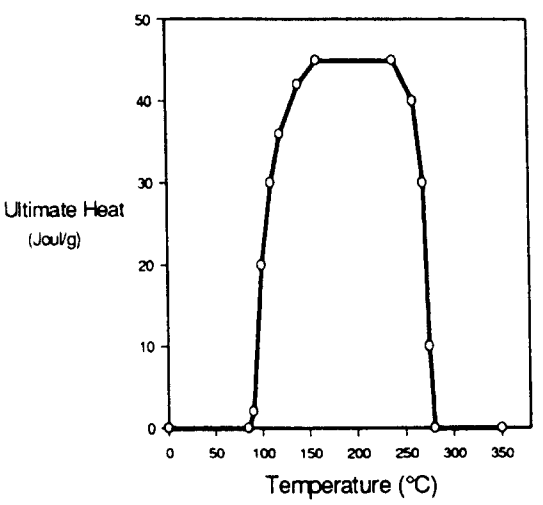


$$\log t_I = \log t_{Ib} + D(T - T_b)^2$$
$$T_b = T_{bq} + \tau E \qquad (9)$$
$$\log t_{Ib} = \log t_{Ibq} - F\tau$$

$$T_{bp} = 190°C$$
$$t_{Ibq} = 10\,s$$
$$D = 1.0 \times 10^{-4} °C^{-2}$$
$$E = 3.0 \times 10^{-5} °C\,cm^2\,dyn^{-1}$$
$$F = 2.6 \times 10^{-6}\,cm^2\,dyn^{-1}$$

(c) rate constant $K$[36,54–58]:

$$\log K = \log K_p - A(T - T_p)^2$$

$$\begin{aligned} T_p &= T_{pq} + \tau B \\ \log K_p &= \log K_{pq} + \tau C \\ T_{pq} &= 190°C \\ K_{pq} &= 0.1\,s^{-1} \\ A &= 4.5 \times 10^{-4} °C^{-2} \\ B &= 3.0 \times 10^{-5} °C\,cm^2\,dyn^{-1} \\ C &= 9.5 \times 10^{7}\,cm^2\,dyn^{-1} \end{aligned} \qquad (10)$$